STEM CELLS AND DEVELOPMENT
Volume 22, Number 13, 2013

DOI: 10.1089/scd.2012.0575

Reconstitution of the Myocardium in Regenerating Newt Hearts is Preceded by Transient Deposition of Extracellular Matrix Components

Tanja Piatkowski,[1,2] Christian Mühlfeld,[2,3] Thilo Borchardt,[1] and Thomas Braun[1]

Adult newts efficiently regenerate the heart after injury in a process that involves proliferation of cardiac muscle and nonmuscle cells and repatterning of the myocardium. To analyze the processes that underlie heart regeneration in newts, we characterized the structural changes in the myocardium that allow regeneration after mechanical injury. We found that cardiomyocytes in the damaged ventricle mainly die by necrosis and are removed during the first week after injury, paving the way for the extension of thin myocardial trabeculae, which initially contain only very few cardiomyocytes. During the following 200 days, these thin trabeculae fill up with new cardiomyocytes until the myocardium is fully reconstituted. Interestingly, reconstruction of the newly formed trabeculated network is accompanied by transient deposition of extracellular matrix (ECM) components such as collagen III. We conclude that the ECM is a critical guidance cue for outgrowing and branching trabeculae to reconstruct the trabeculated network, which represents a hallmark of uninjured cardiac tissue in newts.

Introduction

Ischemic heart disease and heart failure continue to represent major medical challenges worldwide despite intriguing improvements in diagnosis and therapy. Impaired blood perfusion of the myocardium in mammals causes cardiomyocyte cell death and subsequent replacement of the infarcted area by scar tissue [1–3]. Current therapeutic strategies aim to replace the lost tissue by transplantation of cardiomyocytes or cardiac progenitor cells either in engineered tissue grafts or as individual cells. Other approaches are based on stimulation of endogenous repair processes or improved protection of the damaged myocardium. However, current approaches are unlikely to completely restore or regenerate the damaged or lost myocardium, although structural or functional improvement is achievable [4,5].

Interestingly, neonatal mice completely regenerate the heart after amputation of parts of the left ventricle, although the regenerative potential is lost during the first week of life [6]. In contrast, teleosts, such as the zebra fish [7,8] or the Giant danio [9], are able to regenerate cardiac tissue after damage during adult life. So far, all organisms that are capable of extensive cardiac regeneration rely on the initiation of cardiomyocyte proliferation.

Urodele amphibians, such as the newt *Notophthalmus viridescens*, possess remarkable regenerative capacities [10]. Newts regenerate appendages [11–13], the lens [14], and parts of the central nervous system [15]. Previous studies of the amphibian heart regeneration after ventricular apex amputation provided evidence for proliferation of cardiomyocytes and neighboring cells. Changes in the cardiomyocyte morphology included rarefaction and disorganization of myofibrils, decondensation of chromatin, and increased amounts of polyribosomes and rough ER [16]. Initial reports in the newt described only a limited regenerative potential of the heart concomitant with the formation of scar tissue [17–19]. However, more recent studies of heart regeneration after resection of ventricular tissue demonstrated complete regeneration, based on proliferation of cardiac cells and transient upregulation of extracellular matrix (ECM) components during an elongated observation time [20].

The three-dimensional (3D) structures of the newt heart and the cellular processes during the regenerative repatterning of the ventricular trabecular network have not been investigated so far. In particular, a detailed analysis of morphological changes during the process of damage and regeneration is missing. Here, we investigated the cellular fate of cardiac cells in the injury zone, changes in the ultrastructure of the myocardium during the course of regeneration, and the expression and spatial localization of distinct ECM components in a model of mechanical cardiac damage [21]. Our results reveal that reconstitution of the myocardium in regenerating newt

[1]Department for Cardiac Development and Remodelling, Max-Planck-Institute for Heart and Lung Research, Bad Nauheim, Germany.
[2]Institute of Functional and Applied Anatomy, Hannover Medical School, Member of the German Center for Lung Research (DZL), Hannover, Germany.
[3]Institute of Anatomy and Cell Biology, Justus-Liebig-University, Gießen, Germany.

hearts is preceded and possibly directed by transient deposition of ECM components.

Materials and Methods

Animals

Adult red-spotted newts, *Notophthalmus viridescens*, were obtained from Charles Sullivan, Nashville, TN, and were kept in the aquaria at 18°C–20°C and were fed twice a week with gnat larvae. All animal experiments were done in accordance with the Guide for the Care and Use of Laboratory Animals published by the U.S. National Institutes of Health (NIH Publication No. 85–23, revised 1996) and according to the regulations issued by the Committee for Animal Rights Protection of the State of Hessen (Regierungspraesidium Darmstadt).

Injury model

For pain relief, animals were incubated in Butorphanol (0.5 mg/L) from 6 h before until 72 h after cardiac surgery. All invasive interventions were performed under deep anesthesia in a 0.1% MS-222 (Sigma) in a 20-mmol $NaHCO_3$ solution (pH 7.4) for 15–20 min. After incision of the skin and the pericardium, the hearts were fixed in place at the aortic trunk, and the right halve of the ventricle was damaged by repeated orthogonal squeezing with fine forceps. After careful repositioning of the heart into the thoracic cavity, the wound was sealed with Histoacryl (Braun). Animals were disinfected in a sulfamerazin bath (5g/L; Sigma), and transferred into husbandry aquaria after recovery from anesthesia.

Documentation and immunohistochemistry

The injured hearts were investigated either directly or at defined time points after injury and compared with the uninjured control hearts. Anesthetized animals were decapitated before the hearts were excised, transferred to a 60% MEM GlutaMAX medium (Gibco), and imaged with a Stemi SV6 stereomicroscope (Zeiss) and a power shot G6 camera (Canon). Subsequently, the hearts were washed with phosphate-buffered saline (PBS), longitudinally dissected, and fixed with 4% paraformaldehyde for 20 min. Noncardiomyocytes were stained with a Cy3-coupled antibody against Vimentin (1:300/Sigma; C9080) for 2 h at room temperature, followed by F-actin staining with fluorescein isothiocyanate (FITC)-coupled Phalloidin (1:100/Sigma; Art.-Nr. P5282) in a 0.1% Triton X-100 (Carl Roth; Art.-Nr. 3051) solution over night at 4°C. The nuclei were labeled with DAPI (1:1000/Life technologies; Art.-Nr. D3571) for 30 min at room temperature.

For immunofluorescence analysis, the hearts were embedded in an O.C.T. compound tissue-freezing medium and frozen in liquid nitrogen; 16-μm-thick sections were cut with a Leica CM 3000 cryostat, and slices were fixed with 4% paraformaldehyde in PBS. Samples were incubated in a 1:100 dilution of anti-collagen III antibody (Biomol, Art.-Nr. 600-401-105, Hamburg) in 5% bovine serum albumin (SERVA) in PBS overnight at 4°C. As a secondary detection system, an Alexa-Fluor-594-labeled antibody against rabbit (1:500/Life technologies; Art.-Nr. A11012) was used before the sections were stained for F-actin with FITC-coupled Phalloidin (1:100/Sigma; Art.-Nr. P5282) for 45 min at room temperature. Additionally, the nuclei were counterstained with DAPI (1:1000/Life technologies; Art.-Nr. D3571). The images were taken with a Leica TCS SP2 AOBS and processed with Leica Software Suite (Leica) and Adobe CS.

Quantification of the collagen III and F-actin signal

Confocal stacks of injured hearts and hearts without preceded injury, labeled as described above, were analyzed with ImageJ. Therefore, the images were transformed in binary pictures, and the Otsu threshold was used. The ratios of white and black pixels of the collagen III and the F-actin signal were calculated and showed as a diagram using GraphPad Prism 6.

Labeling of damaged cells with the membrane-impermeable dye SYTOX Blue

To analyze the extent of heart injury and removal of damaged cells, the hearts were perfused via the venous system with a SYTOX Blue solution (1:200/Life technologies; S34857) after a preperfusion with PBS. For perfusion, the abdominal wall of deeply anaesthetized animals was opened with a microscissor, and a glass needle was inserted into the caval vein. To control the perfusion process, a second incision of the skin and the pericardium was performed. After final perfusion with PBS to remove the remaining SYTOX Blue, the animals were decapitated. The hearts were removed, transferred to PBS, and imaged with a fluorescence stereomicroscope M205FA (Leica), followed by image postprocessing with Adobe CS.

Transmission electron microscopy

The hearts were fixed in 4% glutaraldehyde, postfixed in osmium tetroxyde, dehydrated, and embedded in Epon. The embedded hearts were cut using an ultramicrotome to generate semi- and ultrathin sections. Semi- and ultrathin sections were stained with toluidine blue or uranyl acetate and lead citrate, respectively. Samples were analyzed using a FEI Morgagni 268 transmission electron microscope. Images were postprocessed with Adobe CS.

Scanning electron microscopy

The hearts were fixed with 1.5% glutaraldehyde and 1.5% paraformaldehyde in 0.15 M Hepes buffer and cut into halves. Afterward, the samples were incubated with 1% osmium tetroxide and dehydrated with 1,2 dimethoxypropan, followed by critical-point drying. The hearts were mounted onto the specimen pod with Leit-C and coated with gold using a sputtering device. The samples were analyzed using a Philips XL30 scanning electron microscope. Images were postprocessed with Adobe CS.

Stereological analysis of the trabeculae volume

Semithin sections of Epon-embedded samples at different time points after injury were prepared and stained with toluidine Blue. Using a computer-assisted stereology system (newCAST; Visiopharm), test fields were obtained by systematic uniform random sampling and overlaid with a point grid. Using the point-counting method, the volume fraction of trabeculae in the ventricle was estimated by

$V_V(\text{trabeculae/ventricle}) = P(\text{trabeculae})/P(\text{ventricle})$ [22]

Statistical analysis

All data were shown in diagrams as mean with standard error of the mean. GraphPad Prism 6 was used for statistical analysis, using one-way analysis of variance, combined with Tukey's multiple comparison test. The differences between time points were considered significant if $P < 0.05$.

Results

The newt heart consists of an atrium, a ventricle, and an aortic trunk. The surface of the heart is covered by melanocytes showing a distinct pattern in different individuals (Fig. 1A). Damage of the right half of the ventricle by repeated squeezing with forceps resulted in a loss of contractions and restricted blood flow in the damaged area covering ca. 50% of the ventricle during early stages after injury (Fig. 1B–D). The first signs of recovery of the damaged region were observed 3 weeks after initial damage (Fig. 1E). Thirty-five days after injury, further improvements were noted as indicated by improved blood flow, which extended to ca. 75% of the ventricle (Fig. 1F). After 84 days, no macroscopic changes were evident between the injured hearts and the control hearts without injury (Fig. 1G–I).

To visualize cells with damaged membranes, SYTOX Blue, a membrane-impermeable nuclear dye, was used (Fig. 2). Immediately after squeezing of 50% of the ventricle with forceps, numerous SYTOX Blue-positive cells were detected (Fig. 2B), which were also apparent 1 day postinjury (dpi) (Fig. 2C). The number of SYTOX Blue-positive damaged cells started to decline at 4 dpi (Fig. 2D). A further reduction was observed at 7 dpi, leading to a complete removal of damaged cells at later stages (Fig. 2E, F).

Cardiomyocytes of trabeculae are normally enveloped by the ECM, which was labeled by immunostaining against collagen III. Collagen III deposition was also detected at the epicardium and the lumen of the myocardium (Fig. 3A, E). Mechanical injury resulted in a severe reduction of F-actin expression in cardiomyocytes already at 1 dpi, which went along with the changes in the staining pattern for collagen III. Increased collagen III deposition was found at the epicardium and the underlying myocardium (Fig. 3B). In addition, collagen III deposition increased around the remaining F-actin-positive cardiomyocytes (Fig. 3F and Supplementary Fig. S1D–F, M; Supplementary Data are available online at www.liebertpub.com/scd). During the following weeks, collagen III levels increased, further resulting in collagen III-positive deposits that crossed the injured region (Fig. 3C, D, G, H). At 35 dpi, the collagen III levels reached their peak (Supplementary Fig. S1G–I, M). The highest concentration was localized around recovered F-actin-positive cardiomyocytes inside the damaged region (Fig. 3I, M). Seven weeks later, the majority of cells in the myocardium regained F-actin expression. Only few patches in the outer myocardium were monitored that lacked F-actin expression, but showed large deposits of collagen III. A high level of collagen III expression was also present at the epicardium (Fig. 3J, N), which did not decline even after 120 days when the myocardium nearly regained the regular morphology (Fig. 3K, O). Full restoration of the myocardium and the epicardium, including resolution of collagen III deposits, was achieved 200 days after initial injury (Fig. 3L, P and Supplementary Fig. S1J–L, M).

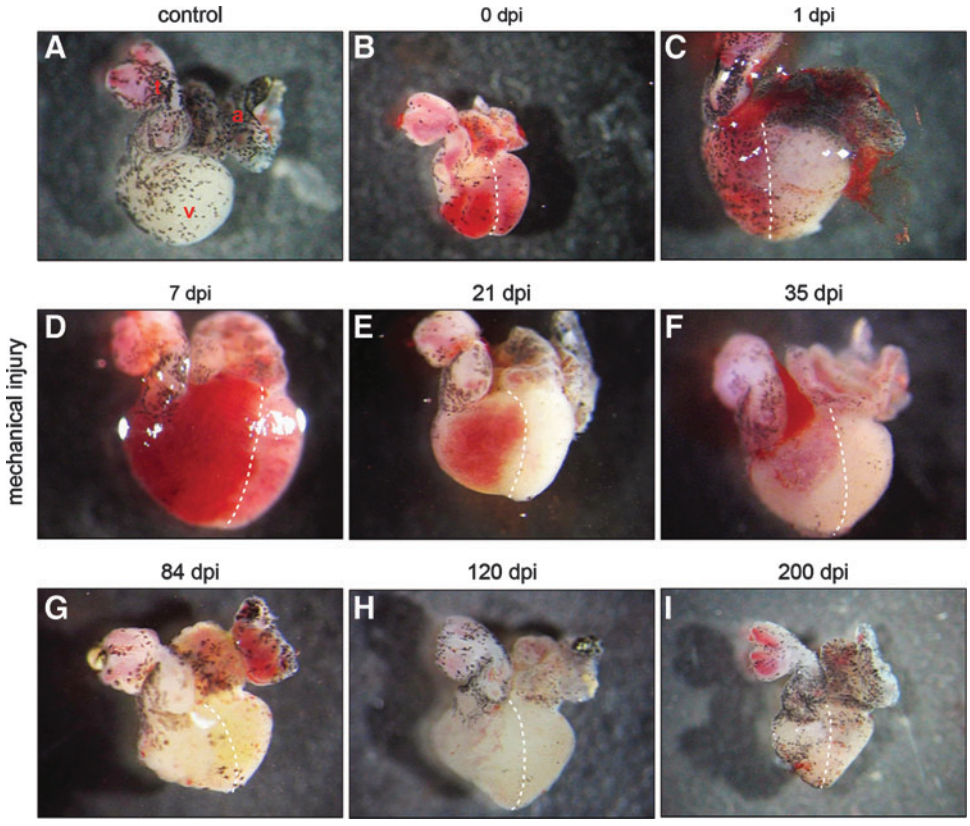

FIG. 1. Macroscopic overview of injured and regenerating newt hearts. **(A)** The newt heart consists of an atrium (a), a ventricle (v), and an aortic trunk (t). The surface is partially covered by melanocytes. **(B)** Immediately after mechanical injury of the right half of the ventricle (0 dpi), the injured region appears red, probably due to restricted blood transport. **(C–E)** Restricted blood flow is visible up to 21 dpi when the size of the injured area decreases. **(F)** Further improvement of the injured area five weeks after damage. **(G–I)** At 84 dpi and afterward, no macroscopic differences between the damaged and undamaged hearts are visible. *Dashed lines* separate the injured from the uninjured region.

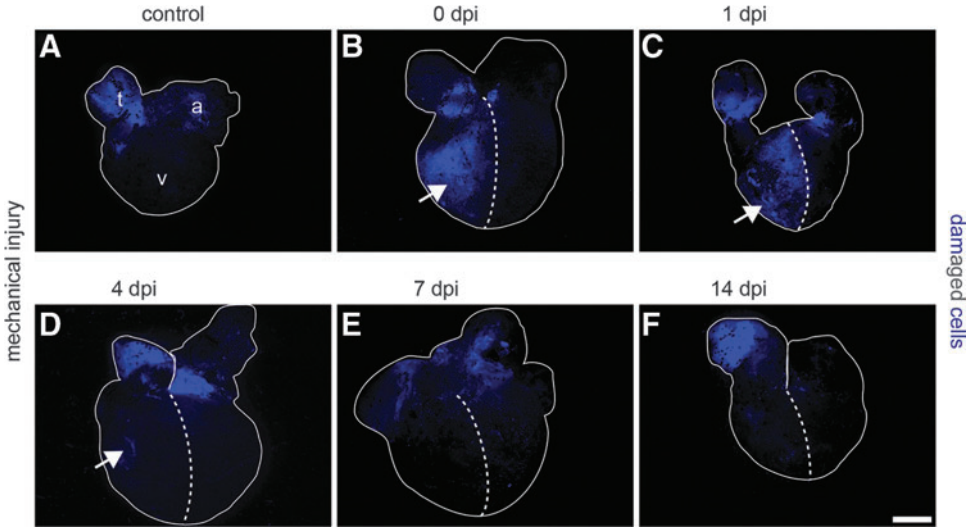

FIG. 2. Mechanical injury of the newt ventricle causes damage of the plasma membranes. The cell membrane-impermeable dye SYTOX Blue stains DNA of cells with damaged membranes. **(A)** Control hearts show no staining of cells in the ventricle (v), but signals in the atrium (a) and the aortic trunk (t), which is caused by preparation artifacts. **(B)** The right half of the ventricle contains numerous SYTOX Blue-labeled cells immediately after injury and one day later **(C)**, indicating a high degree of damage. **(D)** Three days later, only a few SYTOX Blue-labeled cells remain. **(E–F)** After 7 dpi, no SYTOX Blue-labeled cells are present in the injured area anymore. *Dashed lines* separate the injured from the uninjured region; *Arrows* indicate SYTOX Blue-positive cells in the ventricle. Scale bar: 600 μm.

To investigate the effects of mechanical injury and the regeneration process on the 3D organization of heart tissue, scanning electron microscopy analysis in combination with stereological estimation of the trabeculae volumes (Supplementary Fig. S2) was performed at several time points before and after injury (Fig. 4). Undamaged newt hearts displayed a small ventricular lumen and a compact trabeculated myocardium (Fig. 4A, B and Supplementary Fig. S2A). Additionally, intraventricular trabeculae were seen that crossed the ventricle in the middle (Fig. 4A). At 1 dpi, a partial loss of cardiac tissue and a decrease in size of trabeculae in the injured region were visible (Fig. 4C, D and Supplementary Fig. S2B), reflected by reduction of the trabecular volume fraction (Supplementary Fig. S2G). The extent of tissue loss and the size reduction of remaining trabeculae were also visible at 7 dpi, resulting in an uneven surface of remaining trabeculae caused by protruding bodies of subjacent cells (Fig. 4E, F). First alterations were detectable 14 dpi when parts of the trabeculae in the border zone did not display subjacent cells anymore (Fig. 4G, H). One week later, only the outlines of subjacent cells were visible at the surface of the trabeculae, and the injured region was replenished by cardiac tissue, although some gaps in the myocardium were apparent (Fig. 4I, J). The volume fraction of trabeculae steadily increased during this time period, nearly reaching the control values by 35 dpi (Supplementary Fig. S2G). At 120 dpi, the myocardium showed a compact organization, and no significant differences were detected compared to the control hearts (Fig. 4K, L).

To gain further insights into the processes occurring inside trabeculae during heart regeneration, we assembled confocal stacks of control and damaged hearts stained for F-actin and Vimentin at several time points after injury (Fig. 5). The undamaged myocardium showed a compact network of trabeculae consisting of F-actin-positive cardiomyocytes with myofilaments organized in parallel. Cardiomyocytes were enveloped by Vimentin-positive endothelial cells (Fig. 5A, D). One day after injury, the trabeculae inside the damaged region became disrupted, resulting in a partial loss of F-actin-positive cardiomyocytes. The border zone between the damaged and healthy myocardium was characterized by disorganized myofibrils as indicated by diffuse, uneven F-actin staining of cardiomyocytes (Fig. 5B, E). At 7 dpi, F-actin-positive structures were rarefied, although small F-actin-positive processes projected from the border zone into the injured region inside the trabeculae (Figs. C, F). At 14 dpi, a significant increase of F-actin-positive cardiomyocytes was seen, which started to repopulate remaining trabeculae and provided long F-actin-positive processes that crossed the injured region (Fig. 5G, J). Due to continuous repopulation of the damaged region by cardiomyocytes, the majority of trabeculae increased in size and regained myofilaments with regularly arranged F-actin-positive sarcomeres 49 dpi. (Fig. 5H). Interestingly, we also observed a splitting of trabeculae at this stage: Trabeculae divided into two thinner branches, which were both completely covered by Vimentin-positive cells (Fig. 5K). After 200 days, the remaining gaps in the recovering myocardium were filled, and trabeculae contained well-organized cardiomyocytes covered by Vimentin-positive cells (Fig. 5I, L).

We next assessed the ultrastructure of regenerating newt hearts by transmission electron microscopy (TEM) (Fig. 6). The uninjured newt myocardium showed a compact organization of cardiomyocytes inside trabeculae (Fig. 6A) with clearly defined sarcomeres, characterized by the typical pattern of Z-lines, I and M bands, as well as H & A zones (Fig. 6K). Endothelial cells show a flat morphology and elliptic nuclei (Fig. 6G). Only a low number of collagen fibres are present in the interstitial space (Fig. 6T). At 1 dpi, TEM revealed a reduction of cardiomyocytes inside the trabeculae

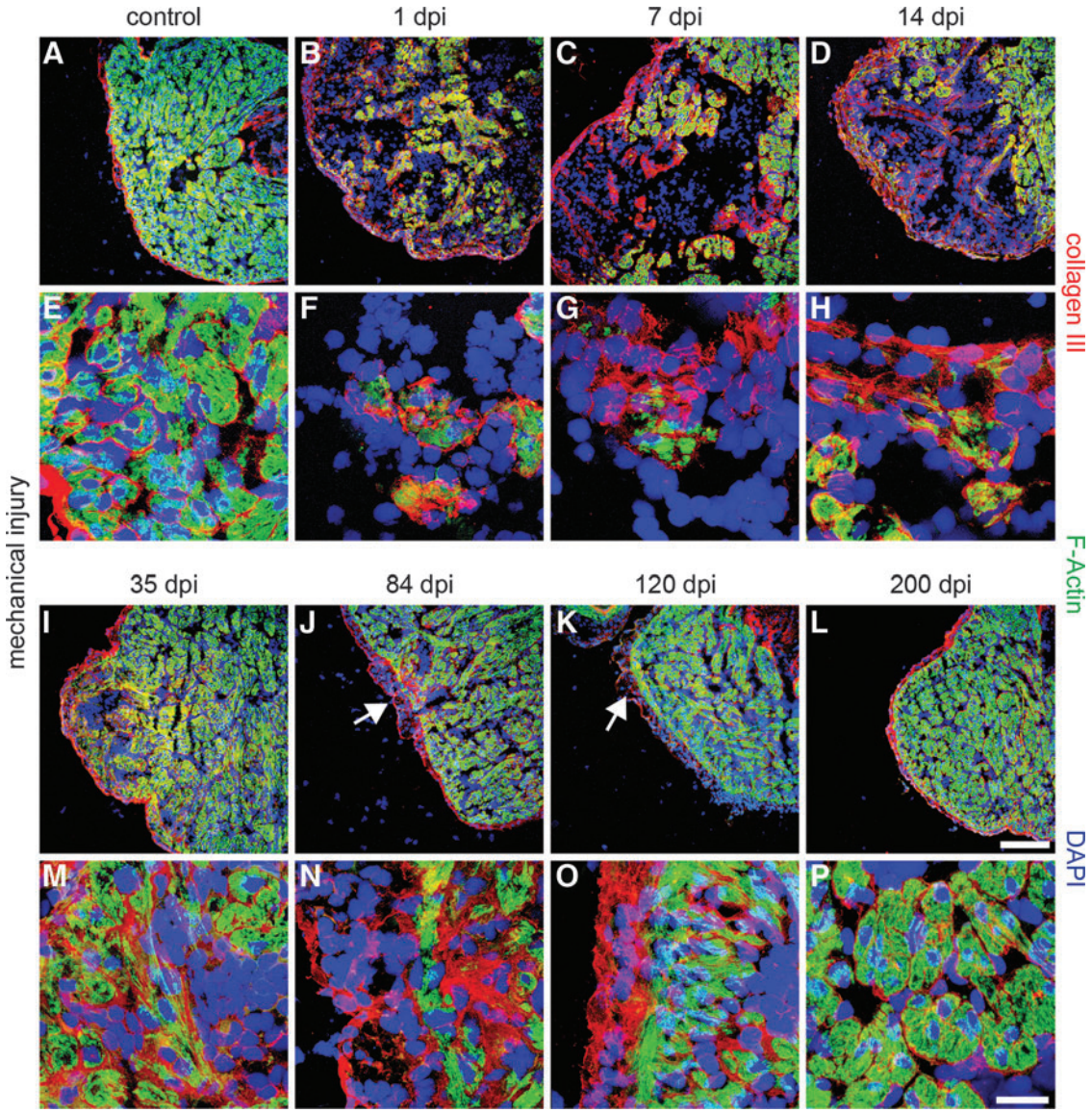

FIG. 3. Increased deposition of extracellular matrix (ECM) during newt heart regeneration. **(A, E)** Control hearts display collagen III immunofluorescence around F-actin-positive cardiomyocytes and underneath the epicardium. Additionally, collagen III covers the ventricular lumen. **(B, F)** Increase of collagen III deposition at the outside of the injured region and around remaining cardiomyocytes at 1 dpi. **(C, D, G, H, I, M)** Collagen III deposits increase up to 35 dpi. Increased signal intensity is obvious around small F-actin-positive patches. **(J, N)** Reduced presence of collagen III after 84 dpi mainly in the outer myocardium. **(K, O)** After 120 dpi, collagen III levels decline with the exception of some deposits at the epicardium and the subjacent myocardium. **(L, P)** At 200 dpi, no significant differences to the control hearts are visible anymore. *Arrows* indicate the regions with higher collagen III levels at 84 and 120 dpi. F-actin: *green*; collagen III: *red*; DAPI: *blue*; scale bar: **(A–D; I–L)** 300 μm; **(E–H; M–P)** 50 μm.

(Fig. 6B). The remaining cardiomyocytes contained necrotic nuclei (Fig. 6Q) and swollen mitochondria with fewer and smaller cristae (Fig. 6R). The organization of sarcomeres was disrupted, and intercalated disks between cardiomyocytes were broken (Fig. 6L). Both cardiomyocytes and endothelial cells suffered from defects in membrane integrity (Fig. 6S). Further, the nuclei of endothelial cells were arched and spherical (Fig. 6H). At 7 dpi, TEM disclosed a decline of the number of cardiomyocytes inside damaged trabeculae (Fig. 6C). Myofibrils of cardiomyocytes in the border zone acquired a fusiform shape without intact Z-lines (Fig. 6M). At 14 dpi, the remaining trabeculae started to fill with cardiomyocytes, although gaps in the myocardium and inside trabeculae were still abundant (Fig. 6D). Some myofibrils inside the border zone contained no Z-lines, but were usually aligned to myofibrils containing Z-lines (Fig. 6N). In contrast to cardiomyocytes, endothelial cells have already regained a normal morphology at this stage with roundup to elliptic-shaped nuclei. Continuous improvement of tissue morphology was monitored between the 5th and 7th week of the regeneration process. The myocardium still showed gaps, but trabeculae were replenished with cardiomyocytes (Fig. 6E) containing normal sarcomeres (Fig. 6O). Despite the normal morphology of regenerated cardiomyocytes, we observed a

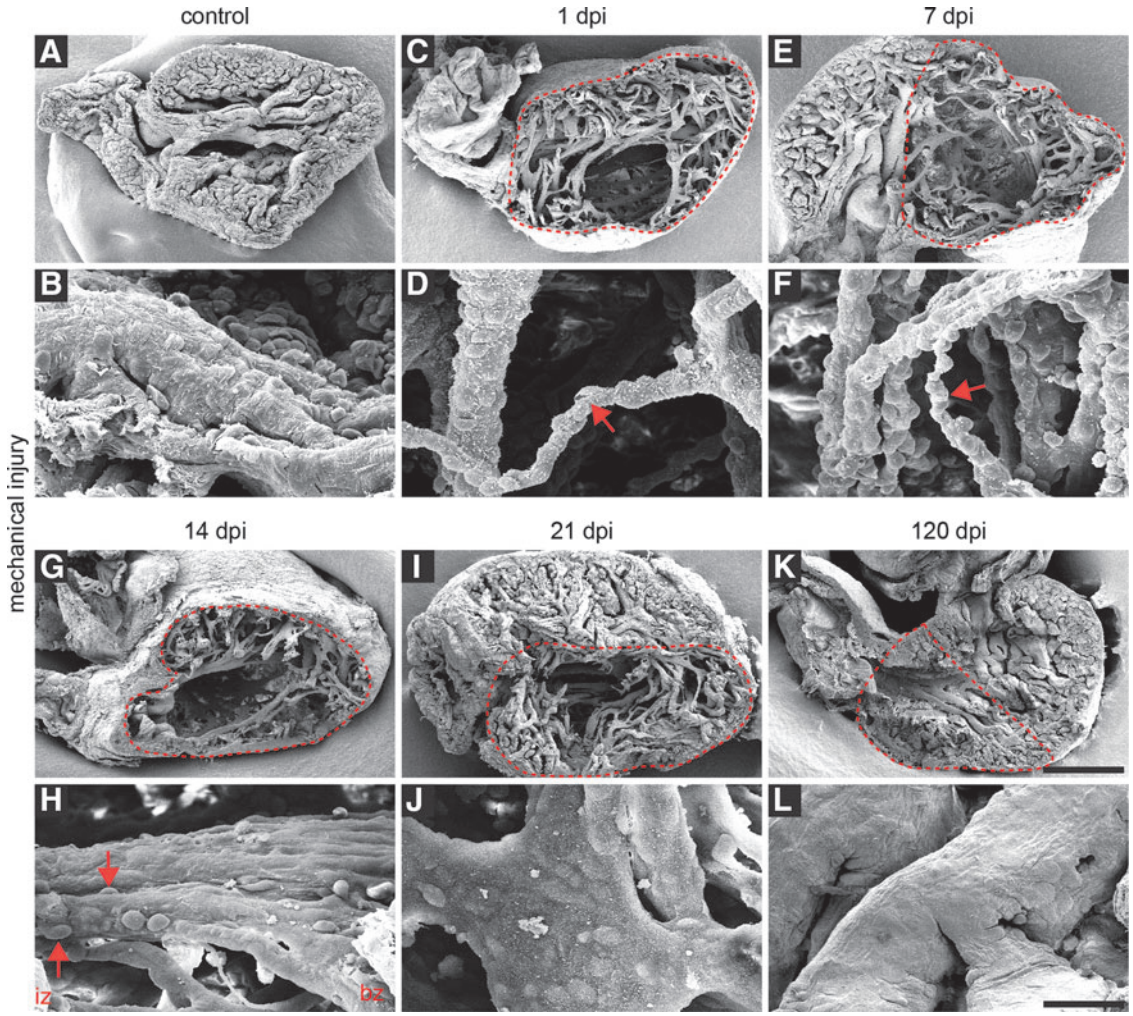

FIG. 4. Large structural defects in the myocardium after mechanical injury. **(A, B)** Scanning electron microscopy analysis of newt hearts reveals a small ventricular lumen and a compact trabeculated myocardium with a smooth surface. Individual trabeculae cross the ventricle. **(C, D)** At 1 dpi, a partial loss of cardiac tissue and a decrease in size of trabeculae in the injured region are apparent. **(E, F)** Large structural defects are visible at 7 dpi. The size of the remaining trabeculae is reduced, exposing the nuclei of subjacent cells (*red arrows* indicate thin trabeculae after 1 and 7 dpi). **(G, H)** At 14 dpi, tissue defects are still apparent. Parts of trabeculae in the border zone (bz) have regained a normal morphology, while the surface of trabeculae in the injured zone (iz) still show off the nuclei of underlying cells (*red arrows* indicate the cells under the surface of trabeculae in the injured region) **(I, J)** At 21 dpi, subjacent cells are still visible at the surface of the trabeculae, but the overall trabecular surface has smoothened. The injured region is replenished with cardiac tissue, but still shows gaps. **(K, L)** At 120 dpi, the myocardium shows a compact organization. No significant differences compared to the control hearts are evident. *Red dashed lines* indicate the injured region; scale bar: **(A, C, E, G, I, K)** 500 μm; **(B, D, F, H, J, L)** 50 μm.

high concentration of collagen fibres in the ECM (Fig. 6U). No significant changes between the regenerated and control hearts were observed by TEM at 200 dpi, marking completion of the regeneration process (Fig. 6F, P, V).

Discussion

Complete regeneration of the newt myocardium within 200 days after mechanical damage

Our detailed morphological assessment of newt heart regeneration revealed that the newt myocardium undergoes complete regeneration within 200 days after mechanical damage, resulting in a complete restoration of the trabecular network of cardiomyocytes covered by endothelial cells [18,23–25] that mainly constitute the newt heart. Moreover, the interstitial area between cardiomyocytes that contains collagen fibrils [23–26], fibroblasts, and nerve fibers [18,23–25] was completely reconstituted. We did not find evidence of interstitial blood vessels within the myocardium similar to previous studies [23–25], indicating that infiltrating cells and nutrients required for regeneration were directly delivered from the ventricular lumen.

Necrotic cell death and not dedifferentiation dominates the first phase of heart regeneration in newts

So far, most studies on the damage and regeneration of the newt heart were based on the removal of cardiac tissue, thus

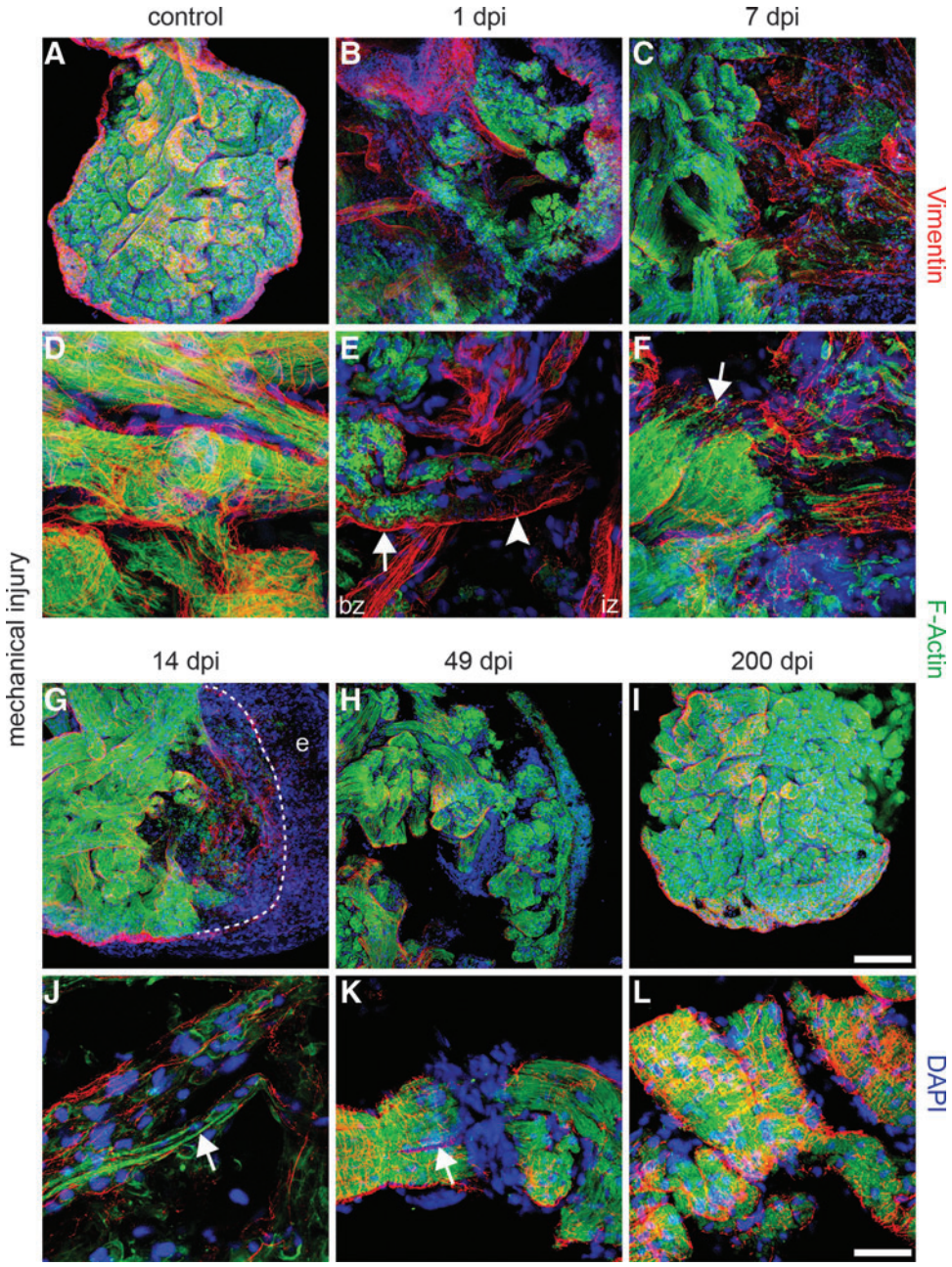

FIG. 5. Repopulation of remaining trabeculae by immature cardiomyocytes. **(A, D)** Immunofluorescence staining of the newt myocardium reveals a compact network of trabeculae filled with F-actin-positive cardiomyocytes and parallel-organized myofilaments. Cardiomyocytes are covered by Vimentin-positive endothelial cells. **(B, E)** At 1 dpi, the injured area contains disorganized trabeculae. Cardiomyocytes in the border zone (bz) shows an irregular pattern of F-actin staining (*arrow*) with partial loss of the F-actin signal inside the remaining trabeculae of the injured zone (iz) (*arrow head*). **(C, F)** Decline of F-actin expression in the iz at 7 dpi. Small F-actin-positive processes project from the border zone into the injured area (*arrow*). **(G, J)** At 14 dpi, the remaining trabeculae fill with F-actin-positive cells containing rare, thin myofibrils (*arrow*). **(H, K)** After 49 dpi, F-actin-positive myofibrils repattern, but gaps in the myocardium are still apparent. Some trabeculae split into two thinner branches, which are both covered by Vimentin-positive cells (*arrow*). **(I, L)** At 200 dpi, regeneration is completed, and the myocardium has regained a compact network of trabeculae with well-organized cardiomyocytes covered by Vimentin-positive cells. F-actin: *green*; Vimentin: *red*; DAPI: *blue*; e: epicardium. Scale bar **A–C** & **G–I**: 300 μm; **D–F** & **J–L**: 50 μm.

limiting insights about the fate of injured cells in vivo [16,18–20,27–29]. We have employed a mechanical damage model that allowed us to analyze the reconstitution of the myocardium in the damaged area. The intense SYTOX Blue staining of the damaged region demonstrated that a large number of cardiac cells experienced severe damage, which was accompanied by a loss of contractile function. Most of the SYTOX Blue stain was removed one week pi, indicating fast and efficient removal of damaged cells, which also resulted in a massive reduction of the size and number of remaining cardiomyocyte-containing trabeculae. Injured cardiomyocytes showed a loss of nuclear membrane integrity, swelling of mitochondria, etc. that are all features of necrotic death [30]. Similarly, endothelial cells showed pronounced fragmentation. Previously, we reported that damaged cardiomyocytes loose the contractile material in response to mechanical injury and concluded that cardiomyocytes primarily undergo dedifferentiation in response to injury [21]. Our new data indicate that dedifferentiation of cardiomyocytes, although present in the border zone of the damaged area, is not the predominant reaction. Instead, damaged cardiomyocytes primarily undergo necrotic cell death and are later replaced by immature cardiomyocytes. This hypothesis is also supported by our scanning electron microscopy data, which revealed large defects devoid of any cellular material in the damaged area when cleared of erythrocytes. At present, it is difficult to judge whether newly forming partially differentiated cardiomyocytes arise from damaged cells or from healthy cardiomyocytes that are recruited into the damaged area by secondary events.

Myocardial regeneration in newts can be divided in three distinct steps

Our study identified three different phases of myocardial regeneration in newts, eventually leading to complete restoration of cardiac structure and function.

Removal of damaged cardiac structures. In the mammalian heart, after myocardial infarction, necrotic cell death is usually accompanied by an inflammatory response, which results in infiltration of the damaged tissue by monocyte-derived macrophages to remove the injured cells [31]. In newts, we detected the first macrophages at the surface of the remaining trabeculae on day 1 pi. The number of macrophages at the trabecular surface decreased at later stages, presumably because of infiltration of macrophages into remaining trabeculae. Simultaneously, with the infiltration by macrophages, the number of SYTOX Blue-positive cells decreased, most likely caused by phagocytosis of necrotic cells inside the trabeculae. The highest levels of SYTOX Blue-positive nuclei were detected directly after injury and 24 h pi just before emergence of macrophages and decreased until 7 dpi. Our data suggest that macrophages are instrumental for the removal of the necrotic cardiomyocytes, which characterizes the first phase of cardiac regeneration in newts.

Rebuilding of a new ECM scaffold. In mammals, myocardial infarction leads to cardiac remodeling, including an upregulation of ECM components, mainly collagens [32–34]. In newts, we found a strong deposition of collagen III within the remaining trabeculae and a strong collagen III expression below the epicardium 1 day after mechanical injury, which presumably stabilizes the damaged region and prevents ventricular rupture [35]. The level of collagen III continuously increased during regeneration and peaked at 35 dpi, when the damaged region became populated by cardiomyocytes and contraction of the myocardium improved. Collagen levels declined only after refilling of trabeculae by cardiomyocytes was completed. This intriguing correlation suggests that deposition of ECM proteins does not only serve a mechanical function but also supply a guidance scaffold for cardiomyocytes, which is well in line with the proposed function of matrix components for tissue reconstitution [36]. The ECM not only is a complex network of fibrillar and nonfibrillar proteins [1,32] providing mechanical support [1,32] but also strongly influences cellular properties [37], including cell adhesion, proliferation, migration, differentiation, and survival [37]. Clearly, the positional information provided by the ECM [1,37] and its content of growth factors and cytokines [37,38] is of utmost importance for tissue regeneration.

Repopulation of the trabecular structures with cardiomyocytes. The ability of the injured newt heart to replace lost cells with new cardiomyocytes has been demonstrated in earlier studies [19–21]. Moreover, it was shown that a certain fraction of newt cardiomyocytes, located within the border zone between the injured and uninjured region, undergoes DNA synthesis and mitosis [18,20,27]. However, the phenotype of proliferating cardiomyocytes is controversially discussed and ranges from highly differentiated cells with intercellular junctions [19] to relatively undifferentiated cells [19–21] with scattered myofilaments [16] or disorganized arrangements of myofilaments [16,18,27]. Our study revealed temporally and spatially distinct morphologies of cardiomyocytes: 1 dpi, we identified cardiomyocytes with a low number of sarcomeres and myofibrils arranged in different directions. At this early time point, numerous cells underwent necrosis in the injured region. Thus, these morphological changes might represent a prelude of damage-induced degradation of cardiomyocytes. At day 7 pi, cardiomyocytes in the border zone showed a relatively normal morphology. Only cardiomyocytes in the injury zone were characterized by a reduction of myofibrils, although most of them already realigned in parallel to the long axis of the trabeculae. Obviously, cardiomyocytes do not need to acquire a high degree of dedifferentiation before initiating DNA synthesis. Similar results were obtained in vitro where cardiomyocytes undergoing cell division only partially lost their normal characteristics [21]. Proliferation of cardiomyocytes within the trabecular was accompanied by smoothing

FIG. 6. Ultrastructural changes of the newt myocardium after mechanical damage. **(A-F)** Transmission electron microscopy analysis of the regenerating myocardium. **(A)** The undamaged myocardium of the ventricle shows compact organization of cardiomyocytes inside the trabeculae. **(B)** At 1 dpi, reduction of cardiomyocytes inside trabeculae is apparent. The majority of damaged cardiomyocytes is removed until 7 dpi **(C). (D)** At 14 dpi, repatterning of ventricular structures has started as indicated by repopulation of the remaining trabeculae with cardiomyocytes. Gaps in the myocardium and inside trabeculae are still visible. At 49 dpi, regeneration led to continuous improvement of tissue morphology. Most trabeculae are populated by cardiomyocytes with only few exceptions **(E). (F)** At 200 dpi, regeneration is completed. No differences between the injured and uninjured hearts are visible. **(G-J)** Morphological alterations of endothelial cells immediately after damage. **(G)** Endothelial cells in the control hearts are flat with elliptic nuclei. **(H)** At 1 dpi, the nuclei of endothelial cells in the injured area are arched and spherical. After 14 dpi, the nuclei of endothelial cells regain a normal round **(I)** to elliptic shape, which is maintained at later stages **(J)**. **(K-P)** Mechanical injury induces massive damage of myofibrils inside cardiomyocytes. **(K)** Myofibrils of the hearts without injury display clearly defined sarcomeres as indicated by the typical pattern of Z-lines, I and M bands, as well as H & A zones. **(L)** Loss of sarcomere integrity and intercalated disks 1 dpi (*red arrow*). **(M)** Fusiform myofibrils without intact Z-lines after 7 dpi. **(N)** Some myofibrils in the border zone contain no Z-lines, although myofibrils are aligned to myofibrils with Z-lines. **(O)** At 49 dpi, myofibrils show a normal morphology despite some gaps in the myocardium. **(P)** Regeneration is complete after 200 dpi. **(Q-S)** Necrosis of different cell types after mechanical injury of the ventricle. **(Q)** At 1 dpi, cardiomyocytes in the injured area contain necrotic nuclei and **(R)** swollen mitochondria with fewer and smaller cristae. **(S)** Membrane integrity of cardiomyocytes and endothelial cells is compromised (indicated by *red arrows*). **(T–V)** Changes in collagen deposition during regeneration. **(T)** The control hearts maintain low levels of collagen fibres in the interstitial space. **(U)** Increasing deposition of collagen fibres until 35 dpi. After 35 dpi, the collagen level drops until normal concentrations are reached at 200 dpi when regeneration is complete (collagen fibres are indicated by *red arrows*) **(V)**. Scale bars: **A–F**: 10 μm; **G–H**: 2 μm; **K–P**: 1 μm; **Q**: 2 μm; **R**: 200 nm; **S**: 500 nm; **T–V**: 1 μm

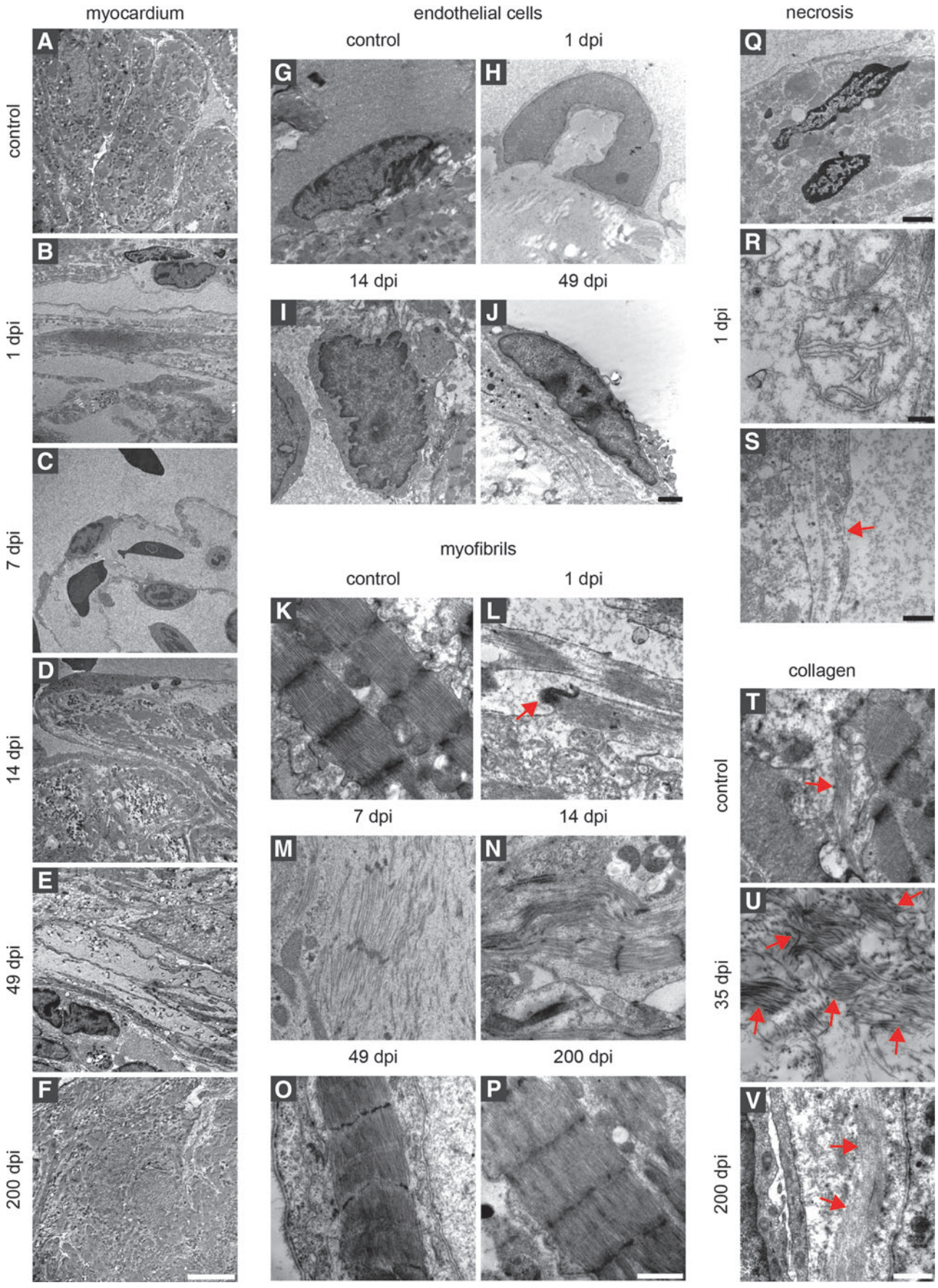
myocardium
control
1 dpi
7 dpi
14 dpi
49 dpi
200 dpi
A
B
C
D
E
F
endothelial cells
control
1 dpi
14 dpi
49 dpi
G
H
I
J
myofibrils
control
1 dpi
7 dpi
14 dpi
49 dpi
200 dpi
K
L
M
N
O
P
necrosis
1 dpi
Q
R
S
collagen
control
35 dpi
200 dpi
T
U
V

of the trabecular surface at 14 dpi, most likely caused by the increasing distance between endothelial cell nuclei, which are pushed apart by the enlarged number of cardiomyocytes within trabeculae.

Day 49 after damage defined a new morphological event: regenerated trabeculae split into two, initially parallel-aligned thinner parts, marking branching of the trabecular network. We reason that repopulation of the remaining trabeculae with cardiomyocytes is not sufficient to reconstitute the 3D architecture of the trabecular network. Hence, it seems essential that new trabeculae form, which is accomplished by splitting and branching. Subsequent maturation of newly formed trabeculae and remodeling of the myocardium were protracted over a relatively long time period (up to 120 day), which was nearly three times longer than the initial reconstitution phase characterized by resorption, proliferation, and morphogenesis. It is tempting to speculate that the need to rapidly regain a preliminary functional state is higher than a complete reversal of the pathogenetic state, which might yield only incremental improvements.

During the course of our study we did not find evidence for the presence of embryonic reserve or undifferentiated cardiomyoblast-like cell types, which is in agreement with previous studies [16,18]. The high plasticity and potential of newt cardiomyocytes to proliferate [21] suggest that the ability of cardiomyocytes to proliferate, even in a partially dedifferentiated state, is sufficient to reconstitute a fully functional myocardium. However, we cannot exclude that newly emerging cardiomyocytes were derived from progenitor cells or a population of partially differentiated, immature cardiomyocytes, although no morphological signs for the existence of such cells in the newt myocardium were obtained. To definitively answer this question, transgenic techniques need to be applied that allow long-term labeling of different cell types and lineage tracing [39,40]. Heart regeneration via proliferation of cardiomyocytes has also been observed in fish [7–9,41–43] and in fetal [44] and neonatal mice [6], suggesting that a stem cell-based mode of heart regeneration was not favored during evolution.

Acknowledgment

The authors wish to thank Sawa Kostin (MPI Bad Nauheim) for embedding the TEM samples. The excellent technical support of Gerhard Kripp and Gerd Magdowski University of Giessen and Christa Lichtenberg MHH for processing the TEM specimens is also highly acknowledged. This work was supported by the DFG [Excellence Cluster Cardio-Pulmonary System (ECCPS), Br1416, and SFB TR81], the German-Israeli Fund, the LOEWE Center for Cell and Gene Therapy, the German Center for Cardiovascular Research, the German Center for Lung Research, and the Universities of Giessen and Marburg Lung Center (UGMLC).

Authors Disclosure Statement

No competing financial interests exist.

References

1. Jourdan-Lesaux C, J Zhang and ML Lindsey. (2010). Extracellular matrix roles during cardiac repair. Life Sci 87: 391–400.
2. Zamilpa R and ML Lindsey. (2010). Extracellular matrix turnover and signaling during cardiac remodeling following MI: causes and consequences. J Mol Cell Cardiol 48:558–563.
3. Nunes SS, H Song, CK Chiang and M Radisic. (2011). Stem cell-based cardiac tissue engineering. J Cardiovasc Transl Res 4: 592–602.
4. Baddour JA, K Sousounis and PA Tsonis. (2012). Organ repair and regeneration: an overview. Birth Defects Res C Embryo Today 96:1–29.
5. Laflamme MA and CE Murry. (2011). Heart regeneration. Nature 473:326–335.
6. Porrello ER, AI Mahmoud, E Simpson, JA Hill, JA Richardson, EN Olson and HA Sadek. (2011). Transient regenerative potential of the neonatal mouse heart. Science 331:1078–1080.
7. Chablais F, J Veit, G Rainer and A Jazwinska. (2011). The zebrafish heart regenerates after cryoinjury-induced myocardial infarction. BMC Dev Biol 11:21.
8. Poss KD, LG Wilson and MT Keating. (2002). Heart regeneration in zebrafish. Science 298:2188–2190.
9. Lafontant PJ, AR Burns, JA Grivas, MA Lesch, TD Lala, SP Reuter, LJ Field and TD Frounfelter. (2012). The giant danio (D. aequipinnatus) as a model of cardiac remodeling and regeneration. Anat Rec (Hoboken) 295:234–248.
10. Brockes J and A Kumar. (2005). Newts. Curr Biol 15: R42–R44.
11. Brockes JP and A Kumar. (2005). Appendage regeneration in adult vertebrates and implications for regenerative medicine. Science 310:1919–1923.
12. Nacu E and EM Tanaka. (2011). Limb regeneration: a new development? Annu Rev Cell Dev Biol 27:409–440.
13. Nye HL, JA Cameron, EA Chernoff and DL Stocum. (2003). Regeneration of the urodele limb: a review. Dev Dyn 226: 280–294.
14. Del Rio-Tsonis K and PA Tsonis. (2003). Eye regeneration at the molecular age. Dev Dyn 226:211–224.
15. Parish CL, A Beljajeva, E Arenas and A Simon. (2007). Midbrain dopaminergic neurogenesis and behavioural recovery in a salamander lesion-induced regeneration model. Development 134:2881–2887.
16. Bader D and J Oberpriller. (1979). Autoradiographic and electron microscopic studies of minced cardiac muscle regeneration in the adult newt, notophthalmus viridescens. J Exp Zool 208:177–193.
17. Becker RO, S Chapin and R Sherry. (1974). Regeneration of the ventricular myocardium in amphibians. Nature 248:145–147.
18. Oberpriller JO and JC Oberpriller. (1974). Response of the adult newt ventricle to injury. J Exp Zool 187:249–253.
19. Bader D and JO Oberpriller. (1978). Repair and reorganization of minced cardiac muscle in the adult newt (Notophthalmus viridescens). J Morphol 155:349–357.
20. Witman N, B Murtuza, B Davis, A Arner, and JI Morrison. (2011). Recapitulation of developmental cardiogenesis governs the morphological and functional regeneration of adult newt hearts following injury. Dev Biol 354:67–76.
21. Laube F, M Heister, C Scholz, T Borchardt and T Braun. (2006). Re-programming of newt cardiomyocytes is induced by tissue regeneration. J Cell Sci 119:4719–4729.
22. Muhlfeld C, JR Nyengaard and TM Mayhew. (2010). A review of state-of-the-art stereology for better quantitative 3D morphology in cardiac research. Cardiovasc Pathol 19:65–82.
23. Hirakow R. (1971). The fine structure of the Necturus (amphibia) heart. Am J Anat 132:401–422.

24. Sommer JR and EA Johnson. (1969). Cardiac muscle. A comparative ultrastructural study with special reference to frog and chicken hearts. Z Zellforsch Mikrosk Anat 98:437–468.
25. Staley NA and ES Benson. (1968). The ultrastructure of frog ventricular cardiac muscle and its relationship to mechanism of excitation-contraction coupling. J Cell Biol 38:99–114.
26. Millhouse EW Jr, JJ Chiakulas and LE Scheving. (1971). Long-term organ culture of the salamander heart. J Cell Biol 48:1–14.
27. Oberpriller J and JC Oberpriller. (1971). Mitosis in adult newt ventricle. J Cell Biol 49: 560–563.
28. Oberpriller JO, JC Oberpriller, AM Arefyeva, VI Mitashov and BM Carlson. (1988). Nuclear characteristics of cardiac myocytes following the proliferative response to mincing of the myocardium in the adult newt, Notophthalmus viridescens. Cell Tissue Res 253:619–624.
29. Oberpriller JO, JC Oberpriller, DG Matz and MH Soonpaa. (1995). Stimulation of proliferative events in the adult amphibian cardiac myocyte. Ann N Y Acad Sci 752:30–46.
30. Kerr JF, GC Gobe, CM Winterford and BV Harmon. (1995). Anatomical methods in cell death. Methods Cell Biol 46:1–27.
31. Frangogiannis NG. (2012). Regulation of the inflammatory response in cardiac repair. Circ Res 110:159–173.
32. Hein S and J Schaper. (2001). The extracellular matrix in normal and diseased myocardium. J Nucl Cardiol 8:188–196.
33. Lindsey ML, J Yoshioka, C MacGillivray, S Muangman, J Gannon, A Verghese, M Aikawa, P Libby, SM Krane and RT Lee. (2003). Effect of a cleavage-resistant collagen mutation on left ventricular remodeling. Circ Res 93:238–245.
34. Lindsey ML, DL Mann, ML Entman and FG Spinale. (2003). Extracellular matrix remodeling following myocardial injury. Ann Med 35:316–326.
35. Sun Y and KT Weber. (2000). Infarct scar: a dynamic tissue. Cardiovasc Res 46:250–256.
36. Badylak SF, DO Freytes and TW Gilbert. (2009). Extracellular matrix as a biological scaffold material: Structure and function. Acta Biomater 5:1–13.
37. Wight TN and S Potter-Perigo. (2011). The extracellular matrix: an active or passive player in fibrosis? Am J Physiol Gastrointest Liver Physiol 301:G950–G955.
38. Weber KT. (1997). Extracellular matrix remodeling in heart failure: a role for *de novo* angiotensin II generation. Circulation 96:4065–4082.
39. Kragl M, D Knapp, E Nacu, S Khattak, M Maden, HH Epperlein and EM Tanaka. (2009). Cells keep a memory of their tissue origin during axolotl limb regeneration. Nature 460: 60–65.
40. Casco-Robles MM, S Yamada, T Miura, K Nakamura, T Haynes, N Maki, K Del Rio-Tsonis, PA Tsonis and C Chiba. (2011). Expressing exogenous genes in newts by transgenesis. Nat Protoc 6:600–608.
41. Jopling C, E Sleep, M Raya, M Marti, A Raya and JC Izpisua Belmonte. (2010). Zebrafish heart regeneration occurs by cardiomyocyte dedifferentiation and proliferation. Nature 464:606–609.
42. Kikuchi K, JE Holdway, AA Werdich, RM Anderson, Y Fang, GF Egnaczyk, T Evans, CA Macrae, DY Stainier and KD Poss. (2010). Primary contribution to zebrafish heart regeneration by gata4(+) cardiomyocytes. Nature 464: 601–605.
43. Schnabel K, CC Wu, T Kurth and G Weidinger (2011). Regeneration of cryoinjury induced necrotic heart lesions in zebrafish is associated with epicardial activation and cardiomyocyte proliferation. PLoS One 6:e18503.
44. Drenckhahn JD, QP Schwarz, S Gray, A Laskowski, H Kiriazis, Z Ming, RP Harvey, XJ Du, DR Thorburn and TC Cox. (2008). Compensatory growth of healthy cardiac cells in the presence of diseased cells restores tissue homeostasis during heart development. Dev Cell 15:521–533.

Address correspondence to:
Tanja Piatkowski
Institute for Functional & Applied Anatomy
Hannover Medical School
OE 4120
Carl-Neuberg-Str. 1
Hannover 30625
Germany

E-mail: piatkowski.tanja@mh-hannover.de

Thomas Braun
Department for Cardiac Development and Remodelling
Max-Planck-Institute for Heart and Lung Research
Ludwigstr. 43
Bad Nauheim 30625
Germany

E-mail: thomas.braun@mpi-bn.mpg.de

Received for publication October 15, 2012
Accepted after revision February 11, 2013
Prepublished on Liebert Instant Online February 11, 2013